Published by :
http://www.ijert.org

International Journal of Engineering Research & Technology (IJERT)
ISSN: 2278-0181
Vol. 8 Issue 12, December-2019

Synthesis and Characterization of Polypyrrole-Antimony (III) Oxide Hybrid Polymer Nanocomposites

Dr. N Dhachanamoorthi[1]
[1]Assistant Professor & Head,
PG Department of Physics, Vellalar College for Women,
Erode, Tamilnadu, India.

Dr. M. Jothi[2]
[2]Assistant Professor,
PG Department of Physics, Vellalar College for Women,
Erode, Tamilnadu, India.

S. Tamilselvan[3]
[3]Assistant Professor of Physics,
Nandha Arts and Science College,
Erode, Tamilnadu, India

***Abstract*-The PPy-Sb_2O_3 nanocomposites with Sb_2O_3 (< 250 nm) nanoparticles various weight percents were prepared by mechanical mixing. Fourier transform infrared (FTIR) spectroscopy, ultraviolet-visible (UV–Vis) spectroscopy, X-ray diffraction (XRD), thermogravimetric analysis (TGA), differential scanning calorimetry (DSC), scanning electron microscopy (SEM), and energy dispersive X-ray analysis spectroscopy (EDAX) were used to characterize the PPy-Sb_2O_3 nanocomposites. The FTIR results indicated that there are some interactions between PPy and Sb_2O_3 nanoparticles. Such an interaction is likely caused by the formation of the coordinate bonding between the lone pair electron of atom in PPy chain with orbit of Sb atom of Sb_2O_3, indicating a reduction in the strength of PPy-Sb_2O_3 interactions as the wt % increases, which may lead to the broader size distribution of Sb_2O_3 nanoparticles dispersed in nanocomposites.**

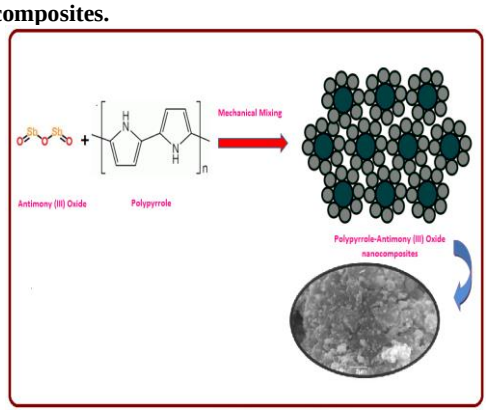

Schematic diagram PPy-Sb_2O_3 nanocomposites

The UV-vis results of PPy-Sb_2O_3 nanocomposites interactions is significantly increased by increasing the Sb_2O_3 wt%, leading to reduce the energy level interval of benzenoid ring and hence result in a red shift. The XRD result indicates that PPy has been successfully anchored on the surface of Sb_2O_3 nPs through the mechanical mixing method. The morphology and elemental composition analysis were characterized by using SEM and EDAX. This result indicates high interaction between PPy and metal oxides.

1. INTRODUCTION

Hybrid inorganic-organic nanocomposite materials have attracted more and more attention due to creating new materials which combine different functions and characteristics of individual materials. Different inorganic materials including carbon nanotubes, metal, metal oxides and nanosheets have been investigated in polymer matrices [1]. Nanocomposite materials have attracted a lot of interest due to their probable commercial exploitation as sensors, batteries, toners in copying machines, quantum electronic devices, smart windows and materials for electromagnetic shielding, etc. Nanocomposite materials made from nanoparticles of oxides and conducting polymers are the most interesting and challenging areas of research in recent times [2]. The conducting polymers, such as polythiophene, polypyrrole (PPy) and polyaniline have been exhaustively studied due to their outstanding mechanical and electrical properties, which afford applications in actuators, sensors and electrochromic devices [3]. Among the conducting polymers, PPy has attracted considerable attention because it is easy synthesis, it has relatively good quality environmental stability and its surface charge characteristics are can be customized by changing the dopant species into the material during the synthesis [4,5]. In the present work, we report the fabrication of conductive PPy-Sb_2O_3 nanocomposites using mechanical mixing method. The chemical structures of the PPy-Sb_2O_3 nanocomposites are characterized by Fourier transform infrared (FT-IR) spectroscopy and optical parameters are by using UV-vis characterization. The thermal stability of the PPy-Sb_2O_3 nanocomposites is performed by thermogravime - tric analysis (TGA) and differential scanning calorimetric (DSC). Scanning electron microscope (SEM) is used to characterize the dispersion of Sb_2O_3 nPs and the morphology of the PPy-Sb_2O_3 nanocomposites. The effects of the Sb_2O_3 nPs on the crystallization structures of the PPy are also studied. In this present work, the inorganic-organic hybrid nanocomposite containing polypyrrole as the organic part and antimony (III) oxide as the inorganic part have been used for studying structural, optical and thermal properties. Such types of nanocomposite have shown to posses small grain size and high stability. To the best of our knowledge, this is the first

International Journal of Engineering Research & Technology (IJERT)
ISSN: 2278-0181
Vol. 8 Issue 12, December-2019

ever attempt made to synthesis and investe of these nanocomposites with special properties.

2. EXPERIMENTAL

2.1. Materials

All of the chemical reagents used in this experiment were A.R. grade. The monomer pyrrole (PPy) and Dodecylbenzene Sulfonic acid (DBSNa) as dopant was purchased from Aldrich Chemical and purified by distillation under reduced pressure, stored in refrigerator before use. Antimony (III) oxide nanopowder, <250 nm nanoparticle (98% purity) from Aldrich Chemical, Ammonium peroxydisulfate (99%, Merck), Ethonal (99% purity, Merck), Acetone (99% purity, Merck) were purchased from Merck chemical. The water used throughout the work is distilled water.

2.2. The preparation of polypyrrole (PPy)

The polypyrrole was synthesized by chemical oxidation polymerization under static condition in a lower temperature. About 900 ml of de ionized water was taken in a flask and an arrangement for mechanical stirring. Dodecylbenzene sulfonic acid solution (DBSNa) as a dopant was dissolved in above 900 ml of deionized water and the solution was well stirred in the flask. Monomer pyrrole was added in the above suspension solution and keeps stirring for 30min. After 30 min ammonium peroxydisulfate $(NH_4)_2S_2O_8$ as an oxidant was added drop wise slowly to the good degree of polymerization is achieved the suspension solution was dark black in color. The entire solution mixture was continuously stirred well at 0-5°C and the reaction was continued for another 24 h over all time speed of rotation maintained at 700rpm. The product was filtered and washed with deionized water, ethanol and acetone, then dried under vacuum at 80°C for 24 h. Experimental setup as shown in Fig.1.

2.3. Synthesis of polypyrrole-Sb_2O_3 nanocomposites

PPy-Sb_2O_3 nanocomposites were synthesized using different wt% of Sb_2O_3 with respect to polypyrrole which are referred as PPy-Sb_2O_3 nanocomposites. Pure PPy was synthesized following the same procedure without Sb_2O_3 nanoparticles. The molar ratio of polymer (PPy) and metal Oxide Sb_2O_3 was 1:0.25 to prepare PPy-Sb_2O_3 (25%) nanocomposites by using mechanical mixing method. Similarly the samples were prepared in the different weight % of Sb_2O_3 nanoparticles like PPy-Sb_2O_3 (50%) and PPy-Sb_2O_3 (100%) by the ratio 1:0.50 and 1:1 respectively.

3. CHARACTERIZATION

FT-IR spectra of the pure PPy, PPy-Sb_2O_3 nanocomposites, Sb_2O_3 nPs samples were recorded at room temperature using FT-IR Spectrometer Make: Perkin Elmer; Model: Spectrum RX 1; Range: 400 cm^{-1}-4000 cm^{-1}; Resolution: 4. The sample was prepared in the pellet form by mixing the polymer powder with KBr by the ratio 1:10 and pressing it in the Perkin Elmer hydraulic device using 15 ton pressure.

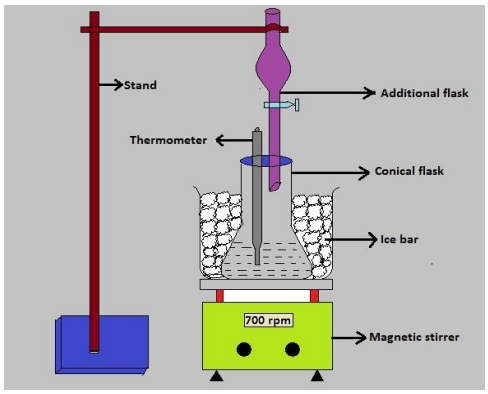

Fig.1 Experimental setup for chemical oxidative polymerization method

UV-vis spectra of the synthesized PPy-Sb_2O_3 nanocomposites powder were determined using a UV–vis spectrometer, Model: Lambda 35; Range: 400 nm-1100 nm; Resolution: 4; Mode of operation: 1.Transmittance (T %) and Absorbance (A %) 2. Reflectance (R %). X-ray diffraction patterns of PPy-Sb_2O_3 nanocomposites samples performed using advance diffractometer with monochromatic CuKα radiation (λ=1.54Å) are used to identify crystalline nature of the samples. The crystallite size was determined from Scherrer relation.

$$D = \frac{K\lambda}{\beta \cos\theta} \qquad (1)$$

where, D is the crystallite size, K is the shape factor for the average crystallite (w0.9), λ is the wavelength of the X-ray which is 1.54 Å for Cu target, B is the full width at half maxima of the crystalline peak in radians, θ is the angle between incident and reflected rays. Thermogravimetric properties of the pure PPy and PPy-Sb_2O_3 nanocomposites were studied in instrument used: STA449 F3 Jupiter; Temperature range: RT to 500 °C; Heating rate: 10K/min; Atmosphere: Nitrogen; Sample Carrier: TG-DSC Sample Carrier; Sample Crucible: TG-DSC Alumina Crucible with lid. The microstructure, size and morphology of the synthesized polypyrrole as well as their dispersity in the PPy-Sb_2O_3 nanocomposites could be determined with the help of scanning electron microscopy (SEM) images were obtained on Make: JEOL; Modal: JSM 6390; Made in Japan. Energy dispersive X- ray spectroscopy employed to analyze the chemical compositions of nanocomposites was carried out using Make: Oxford Instruments; Modal: INCA Pental FET 3; Made in England.

4. RESULT AND DISCUSSION

4.1 FTIR spectral analysis

The FTIR spectra of pure PPy, PPy-Sb_2O_3 (25-100%) nanocomposites and pure Sb_2O_3 nPs are shown in Fig.2. The main transmittance peaks of PPy are appeared at 3402.05 cm^{-1} and 1547.23 cm^{-1} could be corresponded to the N-H stretching vibration and symmetric stretching vibration of C-C bond in the PPy ring, respectively. The band at 1397.53 cm^{-1} is assigned to N-H bending vibration bond. The transmittance

International Journal of Engineering Research & Technology (IJERT)
ISSN: 2278-0181
Vol. 8 Issue 12, December-2019

peaks appeared at 1184.22 cm^{-1} and 905.96 cm^{-1} was attributed to the in-plane bending vibration of C-H bond and the C–H out-of-plane bending vibration indicating the polymerization of pyrrole respectively [6]. The FTIR spectrum of the PPy-Sb_2O_3 (25%) nanocomposite demonstrated the peaks at 3396.57 cm^{-1}, 1545.98 cm^{-1}, 1381.84 cm^{-1}, 1185.86 cm^{-1}, and 908.86 cm^{-1} that are considered to arise from pyrrole ring stretching, N-H stretching vibration, C-C symmetric stretching vibration, N-H bending vibration, C-H in plane bending vibration and C-H out-of-plane bending respectively. The transmittance peaks and corresponding stretching vibration of pure PPy, PPy-Sb_2O_3 nanocomposites was shown in Table.1. These results confirmed the presence of PPy moieties in the nanocomposites. Interestingly, all peak positions shifted towards higher values after Sb ions adsorption. The delocalized π electrons in PPy matrix, which are involved in the skeletal vibration of PPy ring, are affected by the doping ions in the polymer matrix. Different types of dopants in the PPy backbone may disturb the conjugate structure of PPy and this limit the extent of charge delocalization along the polymer chains, leading to red shift. However, as for PPy-Sb_2O_3 nanocomposites, except the peaks of PPy, the broad band between 500 and 950cm^{-1} are attributed to the Sb-O bond, suggesting that the Sb_2O_3 was embedded in PPy matrix. The results indicated that there are some interactions between PPy and Sb_2O_3 particles. Such an interaction is likely caused by the formation of the coordinate bonding between the lone pair electron of atom in PPy chain with orbit of Sb atom of Sb_2O_3, indicating the strength of PPy-Sb_2O_3 interactions, as the wt % increases, which may lead to the broader size distribution of Sb_2O_3 particles dispersed in nanocomposites. Compared to pure PPy, the characteristic peaks of PPy-Sb_2O_3 nanocomposites slightly shifted to higher wavelength, indicating the strong interaction at the interface. Besides, the characteristic peaks of PPy-Sb_2O_3 are well maintained in the nanocomposites, indicating that PPy has been successfully compounded with Sb_2O_3 without changing chemical composition. Comparing to the corresponding peaks of pure PPy, the peaks of PPy-Sb_2O_3 shifted towards lower wavenumber. This shifting of absorption bands may be due to the action of hydrogen bonding between the hydroxyl groups on the surface of Sb_2O_3 nPs and the amine groups in the PPy molecular chains. Similar observations of absorption shifting peaks of PPy-Sb_2O_3 towards are obtained in lower wavenumber. This result indicates that the PPy-Sb_2O_3 nanocomposites have been successful synthesized and the observed shift indicates the interaction between PPy and nPs.

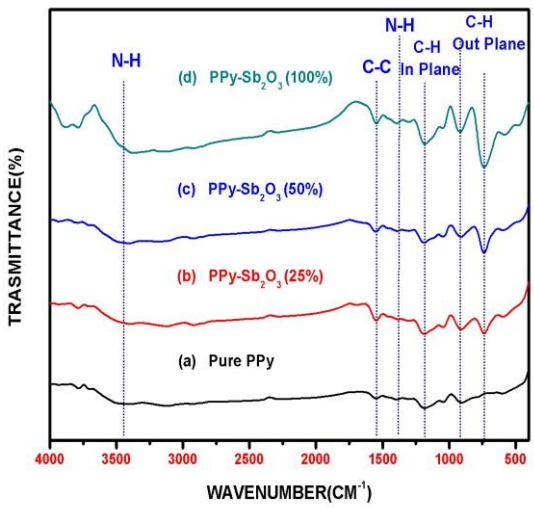

Fig.2 FTIR spectra of pure PPy (a) and PPy-Sb_2O_3 nanocomposites (b, c & d)

Sample Name	N-H stretching vibrations (cm^{-1})	C–C ring symmetric stretching vibrations (cm^{-1})	N-H bending vibrations (cm^{-1})	In-plane C–H bending Vibrations (cm^{-1})	Out-plane C–H bending Vibrations (cm^{-1})
Pure PPy	3402.05	1547.23	1397.53	1184.22	905.96
PPy-Sb_2O_3 (25%)	3396.57	1545.98	1381.84	1185.86	908.86
PPy-Sb_2O_3 (50%)	3410.94	1548.74	1387.97	1187.47	911.61
PPy-Sb_2O_3 (100%)	3373.71	1544.73	1395.43	1181.12	916.23

Table.1 FTIR data of pure PPy and PPy-Sb_2O_3 nanocomposites

4.2. UV-vis absorption spectral analysis

The UV-vis spectra of pure PPy (a), PPy-Sb_2O_3 (b,c, d) nanocomposites and pure Sb_2O_3 (e) are shown in Fig.3. The absorption reveals that there is different composition and morphology in ranging Sb_2O_3 concentration from 25-100% in PPy-Sb_2O_3 nanocomposites. However, as the characteristic absorption bands of pure PPy are obtained in the wavelengths range of 250-300 nm, 450-450 nm and 900-1000 nm. UV-vis analysis was also conducted to analyze the PPy are presented in Fig.4 (a), in which the intermediates exhibit an absorption band appeared at about 473nm. This band is due to the formation of phenazine-like structures in this stage. These bands are assigned to the formation of PPy. The first absorption band corresponds to the π-π* electron transition within benzenoid segments. The second and the third bands correspond to the doped state and the polaron formation in PPy respectively. From the spectroscopic and theoretical data indicate, that the absorption band at 400-500 nm (4-3 eV) is assigned to π-π* transition of PPy. The band gap of each case is determined from Tauc plot which is shown in Table.2.

International Journal of Engineering Research & Technology (IJERT)
ISSN: 2278-0181
Vol. 8 Issue 12, December-2019

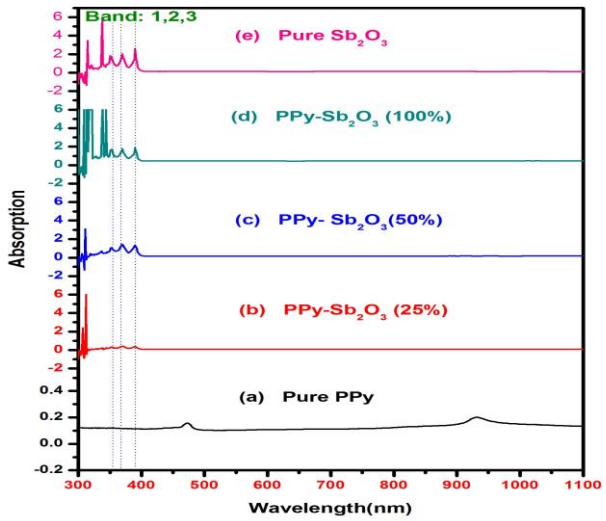

Fig.3 UV-vis spectra of pure PPy (a), PPy-Sb_2O_3 nanocomposites (b, c, d) and pure Sb_2O_3 nPs

Sample Name	Wavelength (nm)			Absorption			Band gap (eV)
	Band: 1	Band: 2	Band: 3	Band: 1	Band: 2	Band: 3	
Pure PPy	260	473	931	0.1826	0.1581	0.2017	3.46
PPy-Sb_2O_3 (25%)	343	360	379	0.3393	0.4155	0.3951	3.04
PPy-Sb_2O_3 (50%)	342	359	379	1.0751	1.4434	1.3211	1.76
PPy-Sb_2O_3 (100%)	343	359	380	1.7405	1.7130	1.8569	1.49
Pure Sb_2O_3	340	359	380	1.8181	2.0666	2.5913	1.71

Table.3 Crystallographic parameters of pure PPy, PPy-Sb_2O_3 nanocomposites and pure Sb_2O_3 nPs

Among the various cases, the highest band gap energy was obtained for pure PPy and then the band gap was decreased with increasing Sb_2O_3 concentration which is clearly shown in the Table.2. The PPy-Sb_2O_3 interactions is significantly increased by increasing the Sb_2O_3 wt%, leading to reduce the energy level interval of benzenoid ring and hence, result in a red shift. The FTIR spectra of the nanocomposites shown in Fig.3 also support this conclusion. Upon doping PPy exhibits unusual electronic structure due to electron–phonon coupling. Polarons and bipolarons states appear within the band gap, which gives rise to the broad band at wave length 900-1000 nm in the case of pure PPy. Generally, the optical band gap in a semiconductor is determined by plotting absorption coefficients (α) as $(\alpha h\nu)^{1/m}$ vs. hν where 'm' represents the nature of the transition and hν is the photon energy. Now 'm' may have different values, such as $\frac{1}{2}$, 2, $\frac{3}{2}$ and 3 for allowed direct, allowed indirect, forbidden direct and forbidden indirect transitions respectively.

$$\alpha = \frac{A(h\nu - E_g)^{\frac{1}{2}}}{h\nu} \longrightarrow (1)$$

where 'A' is the absorption constant for a direct transition. For allowed direct transition one can plot $(\alpha h\nu)^2$ vs. hν as shown in Fig.4 and extrapolate the linear portion of it to α=0 value to obtain the corresponding band gap.

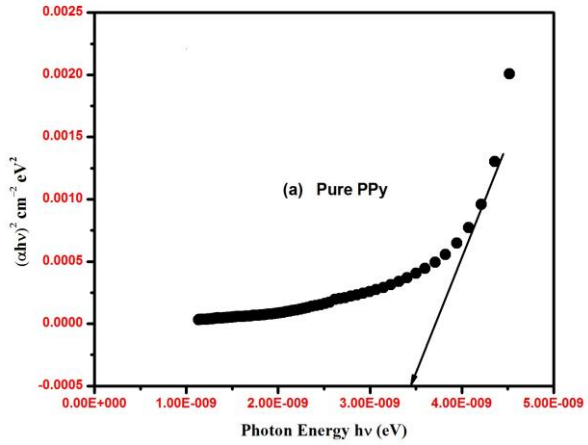

Fig.4a

The optical absorption coefficient (α) near the absorption edge for direct interband transitions is given by the equation (1). The band gap of PPy with antimony concentration implies that electronic structure of PPy is affected [8,9]. UV-Vis spectral data and the band gap of pure PPy, PPy-Sb_2O_3 (25-100%) nanocomposites and pure Sb_2O_3 are as shown in Table.2.

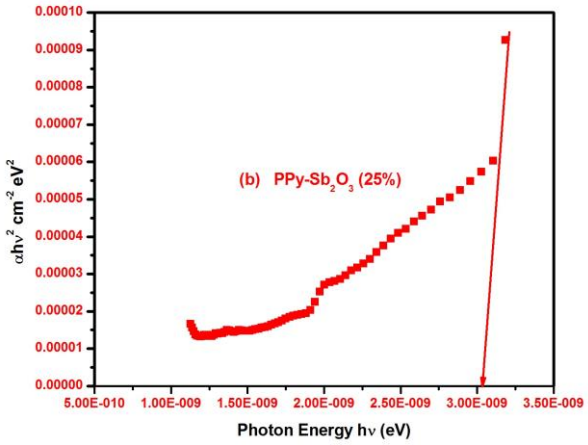

Fig.4b

International Journal of Engineering Research & Technology (IJERT)
ISSN: 2278-0181
Vol. 8 Issue 12, December-2019

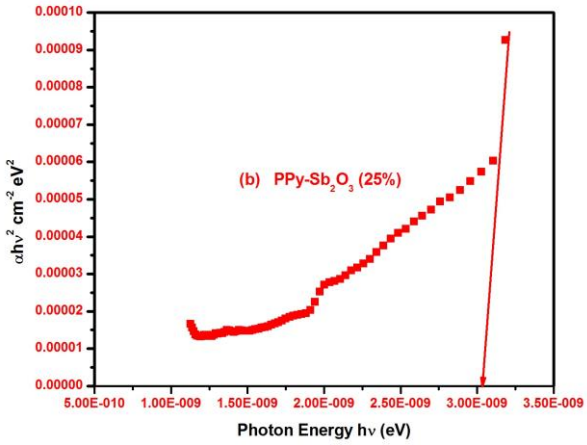

Fig.4c

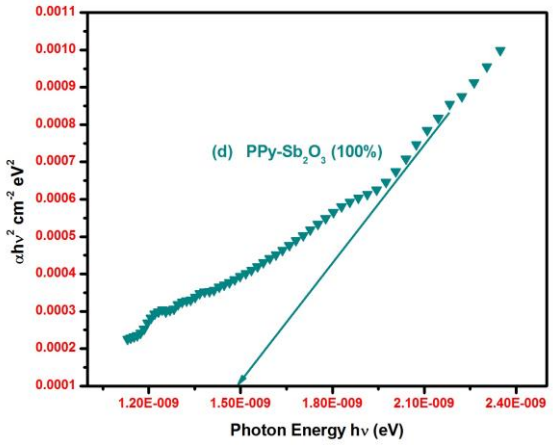

Fig.4d

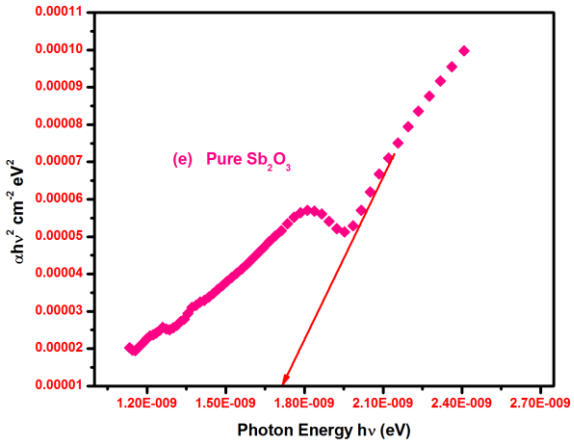

Fig.4d

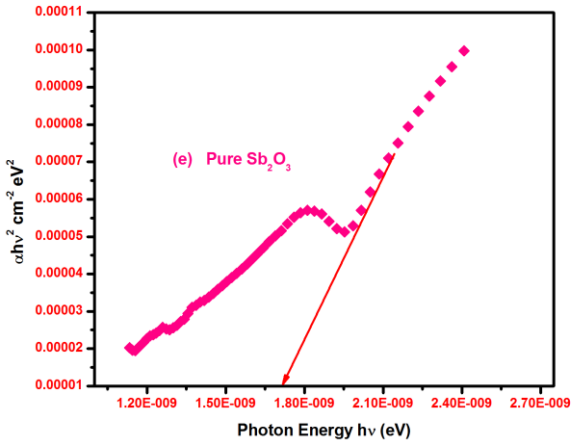

Fig.4e

Fig.4a-4e Tauc plot for $(\alpha h\nu)^2$ vs hν of pure PPy, PPy-Sb_2O_3 nanocomposites and pure Sb_2O_3 nPs

4.3. X-Ray diffraction studies

Fig.5 shows the XRD patterns of pure PPy, PPy-Sb_2O_3 nanocomposites (25-100%) and pure Sb_2O_3 nPs which is a evidence of crystalline nature of the samples. The XRD pattern of pure PPy shows a broad peak and sharp peak appeared at 23.04° and 44.36° respectively, which indicates the crystalline nature. XRD curve of PPy shows that the PPy prepared in the absence of Sb_2O_3 nPs is amorphous in nature. The crystallite sizes of the PPy were estimated from X-ray line broadening using Scherer's formula. It can be seen clearly from the XRD patterns of Sb_2O_3 nPs, that the Sb_2O_3 nPs showed a single-phase in nature. There was no secondary phase detected and the high intensity of the peaks revealed the crystalline nature of the as Sb_2O_3 nPs. Obviously, the diffraction peaks of the Sb_2O_3 nPs appear in the PPy-Sb_2O_3 nanocomposites from the Fig.5 (b,c,d) the intensity of these peaks becomes stronger with increasing the nanoparticle loadings, while the two original peaks of PPy show a reduced intensity at 2θ=23.04 and 44.36°. The XRD pattern also confirm the presence of antimony in the PPy-Sb_2O_3 (25-100%) nanocomposites and pure Sb_2O_3 the crystallize size as-calculated, where the average crystallize size are 97 nm (25%), 170 nm (50%), 176 nm (100%) and 152 nm (pure Sb_2O_3). The strain and dislocation density of pure PPy, PPy-Sb_2O_3 nanocomposites (25-100%), pure Sb_2O_3 nPs data are seen in Table.3. The parameters are slightly changed with the addition of Sb_2O_3 nPs. Furthermore, these results revealed the amorphous nature of PPy in the nanocomposites, suggesting that the addition of Sb_2O_3 nPs retain the crystallization of the PPy molecular chains. This may be because when PPy is adsorbed on the surface of the Sb_2O_3 nPs. The increasing trend intensity indicating that the Sb_2O_3 greatly increased due to the adsorption of PPy molecular chains on the surface of the Sb_2O_3 nPs. In order to study the effect of the addition of Sb_2O_3 nPs in PPy matrix, a careful analysis of the position of the XRD peak indicates that, there is a shifting in peak's position towards lowering 2θ value, but in this case, the crystallinity of Sb_2O_3 nPs was found to be disturbed in the PPy-Sb_2O_3 nanocomposites. However, in the present work the crystallinity of Sb_2O_3 is not disturbed by PPy

International Journal of Engineering Research & Technology (IJERT)
ISSN: 2278-0181
Vol. 8 Issue 12, December-2019

molecular chain on the surface of Sb_2O_3 nPs as can be seen from Fig.6. The shifting of the peak's position clearly indicates that PPy-Sb_2O_3 nanoparticles are incorporating into the PPy polymer matrix. The broad weak diffraction peak of PPy still exists, but its intensity decreases. This indicates a strong effect of the Sb_2O_3 nPs on the structures of crystalline of the formed PPy and the interaction between PPy backbone and Sb_2O_3 nPs.

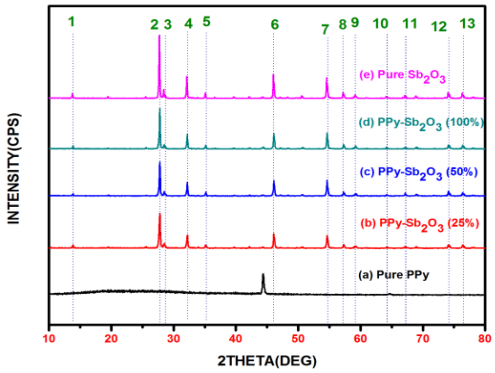

Fig.5 X-Ray diffraction patterns of pure PPy (a), PPy-Sb_2O_3 nanocomposites (b, c, d) and pure Sb_2O_3 nPs (e)

This result indicates that, PPy has been successfully anchored on the surface of Sb_2O_3 NPs through the mechanical mixing method. However, the characteristic peak intensities of PPy-Sb_2O_3 nanocomposite gradually decreased with increasing the weight percentage of Sb_2O_3, indicating the incorporation of Sb_2O_3 into the polymer matrix. Previous literature also support that the parent work that the introduction of Sb_2O_3 will affect the crystalline behavior of PPy [10-12].

	Pure PPy						
	2θ	**FWHM**	**Intensity**	**d Spacing Value**	**Crystallize size (nm)**	**Strain**	**Dislocation density**
1	23.04	0.071	263	3.8570	114	0.0006	$1.30*10^{-14}$
2	44.36	0.094	980	2.0404	91	0.0004	$8.32*10^{-15}$
Peak No	**PPy-Sb_2O_3 (25%)**						
	2θ	**FWHM**	**Intensity**	**d Spacing Value**	**Crystallize size (nm)**	**Strain**	**Dislocation density**
1	13.88	0.118	130	6.3749	67	0.0018	$0.20*10^{-15}$
2	27.80	0.118	1647	3.2065	69	0.0009	$4.80*10^{-15}$
3	28.52	0.118	220	3.1271	69	0.0009	$4.80*10^{-15}$
4	32.22	0.165	610	2.7760	50	0.0001	$2.50*10^{-15}$
5	35.20	0.071	140	2.5475	117	0.0004	$1.37*10^{-14}$
6	46.10	0.118	570	1.9673	73	0.0005	$5.34*10^{-15}$
7	54.64	0.071	617	1.6783	125	0.0002	$1.58*10^{-14}$
8	57.26	0.118	170	1.6076	76	0.0004	$5.87*10^{-15}$
9	59.14	0.071	103	1.5609	128	0.0002	$1.65*10^{-14}$
10	64.14	0.118	57	1.4507	79	0.0003	$6.30*10^{-15}$
11	68.96	0.071	77	1.3606	135	0.0002	$1.84*10^{-14}$
12	74.08	0.071	163	1.2787	140	0.0001	$1.96*10^{-14}$
13	76.44	0.071	170	1.2450	142	0.0001	$2.02*10^{-14}$
Peak No	**PPy-Sb_2O_3 (50%)**						
	2θ	**FWHM**	**Intensity**	**d Spacing Value**	**Crystallize size (nm)**	**Strain**	**Dislocation density**
1	14.00	0.047	213	6.3205	170	0.0007	$2.89*10^{-14}$
2	27.94	0.047	1747	3.1907	174	0.0003	$3.03*10^{-14}$
3	28.76	0.047	113	3.1016	174	0.0003	$3.04*10^{-14}$
4	32.34	0.071	567	2.7659	116	0.0004	$1.35*10^{-14}$
5	35.28	0.071	153	2.5419	117	0.0004	$1.37*10^{-14}$
6	46.24	0.071	607	1.9617	121	0.0003	$1.47*10^{-14}$
7	54.80	0.047	533	1.6738	190	0.0001	$3.62*10^{-14}$
8	57.42	0.047	173	1.6035	192	0.0001	$3.71*10^{-14}$
9	59.32	0.071	110	1.5566	128	0.0002	$1.65*10^{-14}$
10	64.28	0.047	83	1.4479	199	0.0001	$3.98*10^{-14}$
11	69.04	0.047	80	1.3593	205	0.0001	$4.20*10^{-14}$
12	74.20	0.047	153	1.2770	211	0.0001	$4.48*10^{-14}$
13	76.60	0.047	103	1.2428	215	0.0001	$4.63*10^{-14}$
Peak No	**PPy-Sb_2O_3 (100%)**						
	2θ	**FWHM**	**Intensity**	**d Spacing Value**	**Crystallize size (nm)**	**Strain**	**Dislocation density**
1	13.88	0.047	153	6.3749	170	0.0007	$2.89*10^{-14}$
2	27.80	0.047	1907	3.2065	174	0.0003	$3.02*10^{-14}$

International Journal of Engineering Research & Technology (IJERT)
ISSN: 2278-0181
Vol. 8 Issue 12, December-2019

3	28.48	0.047	210	3.1314	174	0.0003	$3.03*10^{-14}$
4	32.20	0.047	713	2.7776	175	0.0003	$3.09*10^{-14}$
5	35.26	0.047	107	2.5433	177	0.0002	$3.14*10^{-14}$
6	46.10	0.047	733	1.9673	183	0.0002	$3.37*10^{-14}$
7	54.30	0.047	47	1.6880	189	0.0001	$3.60*10^{-14}$
8	57.28	0.094	220	1.6071	96	0.0003	$9.26*10^{-15}$
9	59.20	0.047	140	1.5595	194	0.0001	$3.77*10^{-14}$
10	64.38	0.047	53	1.4459	199	0.0001	$3.98*10^{-14}$
11	68.90	0.047	87	1.3617	203	0.0001	$4.19*10^{-14}$
12	74.10	0.071	183	1.2784	140	0.0001	$1.96*10^{-14}$
13	76.32	0.047	123	1.2467	214	0.0001	$4.61*10^{-14}$
Peak No	**Pure Sb_2O_3**						
	2θ	**FWHM**	**Intensity**	**d Spacing Value**	**Crystallize size (nm)**	**Strain**	**Dislocation density**
1	13.80	0.047	253	6.4117	170	0.0007	$2.89*10^{-14}$
2	27.72	0.118	2957	3.2155	69	0.0009	$4.80*10^{-15}$
3	28.42	0.071	430	3.1379	115	0.0005	$1.33*10^{-14}$
4	32.10	0.094	1037	2.7861	87	0.0006	$7.72*10^{-15}$
5	35.06	0.047	273	2.5573	177	0.0002	$3.13*10^{-14}$
6	46.02	0.094	1130	1.9760	91	0.0004	$8.42*10^{-15}$
7	54.56	0.047	980	1.6806	190	0.0001	$3.61*10^{-14}$
8	58.84	0.047	67	1.5681	193	0.0001	$3.76*10^{-14}$
9	59.14	0.071	180	1.5609	128	0.0002	$1.65*10^{-14}$
10	64.10	0.071	90	1.4516	131	0.0002	$1.74*10^{-14}$
11	67.22	0.047	70	1.3916	202	0.0001	$4.11*10^{-14}$
12	74.04	0.047	263	1.2793	211	0.0001	$4.47*10^{-14}$
13	76.24	0.047	103	1.2478	214	0.0001	$4.61*10^{-14}$

Table.3 Crystallographic parameters of pure PPy, PPy-Sb_2O_3 nanocomposites and pure Sb_2O_3 nPs

4.4. Thermogravimetric analysis

The thermogravimetric analysis of pure PPy, PPy-Sb_2O_3 (25-100%) nanocomposites and pure Sb_2O_3 nPs is shown in Fig.6. To investigate the weight loss of the as-synthesized pure PPy, PPy-Sb_2O_3 (25-100%) nanocomposites and pure Sb_2O_3 nPs samples, the thermogravimetric analysis has been carried out in a nitrogen atmosphere. In order to see the effect of temperature on the thermal behavior of the polymer thermogravimetric analysis of PPy-Sb_2O_3 nanocomposites has been carried out from 25-500 °C temperature. To investigate the thermal properties and the interaction between PPy and Sb_2O_3, TGA analysis has been carried out through decomposition curve. From the Fig.6 (a) pure PPy undergoes two-step decompositions are observed. The first one is appeared at 110 °C which is due to the removal of adsorbed water resulting with a weight loss of 53.99%. The second step of decomposition starts from 200 °C and goes up to 450 °C with about 26.31% weight loss. Finally the residual mass and residual temperature of pure PPy is 19.70 and 497.8 °C. Degradation of PPy-Sb_2O_3 (25%) nanocomposite takes place in five steps. The first three steps of weight loss observed at 200 °C is due to the removal of adsorbed water and the remaining second step (between 200 °C and 450 °C) of weight loss is due to the breakdown of the polymer backbone in the nanocomposites as shown in Fig. 7 (b).

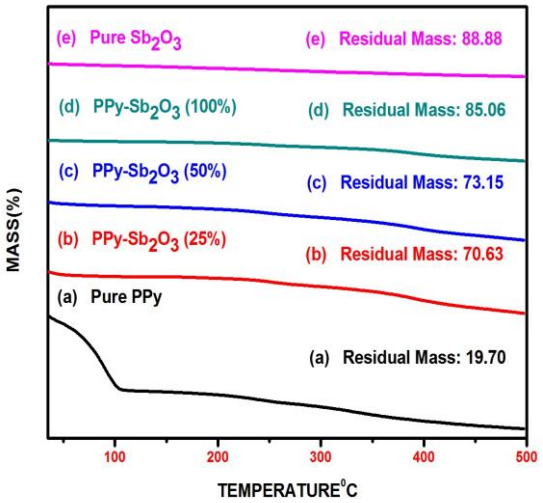

Fig.6 TGA spectra of pure PPy (a), PPy-Sb_2O_3 nanocomposites (b,c,d) and pure Sb_2O_3 nPs (e)

Pure PPy			
Mass Change	**Mass**	**Residual Mass**	**Residual Temp**
Stage: 1	-53.99	19.70	497.80
Stage: 2	-26.31		
Stage: 3	-		
Stage: 4	-		
Stage: 5	-		
PPy-Sb_2O_3 (25%)			
Mass Change	**Mass**	**Residual Mass**	**Residual Temp**

International Journal of Engineering Research & Technology (IJERT)
ISSN: 2278-0181
Vol. 8 Issue 12, December-2019

Stage: 1	-3.07	70.63	497.70
Stage: 2	-2.02		
Stage: 3	-4.03		
Stage: 4	-4.31		
Stage: 5	-15.94		
PPy-Sb_2O_3 (50%)			
Mass Change	**Mass**	**Residual Mass**	**Residual Temp**
Stage: 1	-3.21	73.15	498.00
Stage: 2	-1.97		
Stage: 3	-4.32		
Stage: 4	-3.73		
Stage: 5	-13.62		
PPy-Sb_2O_3 (100%)			
Mass Change	**Mass**	**Residual Mass**	**Residual Temp**
Stage: 1	-1.23	85.06	497.08
Stage: 2	-0.43		
Stage: 3	-1.62		
Stage: 4	-1.59		
Stage: 5	-2.08		
Stage: 6	-7.99		
Pure Sb_2O_3			
Mass Change	**Mass**	**Residual Mass**	**Residual Temp**
Stage: 1	-3.41	88.88	497.90
Stage: 2	-3.51		
Stage: 3	-4.20		
Stage: 4	-		
Stage: 5	-		
Stage: 6	-		

Table.4 TGA parameters of pure PPy, PPy-Sb_2O_3 nanocomposites and pure Sb_2O_3 nPs

The residual mass and residual temperature of PPy-Sb_2O_3 (25%) nanocomposite is 70.63 and 497.7 °C respectively. Mass changes, residual mass, residual temp of pure PPy, PPy-Sb_2O_3 (25-100%) nanocomposites and pure Sb_2O_3 nPs are shown in Table.4.The mass change of PPy-Sb_2O_3 (25-100%) nanocomposites have five stages of weight loss are obtained for this nanocomposites while the spectrum pure Sb_2O_3 nPs have two weight loss appeared in which the weight loss is decreased with increasing Sb ion concentration and the residual mass of PPy-Sb_2O_3 (25-100%) nanocomposites are 70.63 (25%), 73.15 (50%), 85.06 (100%). This data clearly reveals the residual mass are increased Sb ion content and with have constant residual temperature [13,14]. By comparing the thermo graphs of synthesized are pure PPy and nanocomposites, one can be understood, the different thermal behavior of the materials. The residual mass increased with the ionic concentration of Sb_2O_3 in PPy-Sb_2O_3 nanocomposite materials. These results show that the PPy-Sb_2O_3 nanocomposites materials have remarkable improvement in thermal stability. These results confirm the strong interaction between polypyrrole and Sb_2O_3 forming a stable nanocomposites.

4.5. Differential scanning calorimetric analysis

Differential scanning calorimetric spectrum of pure PPy, PPy-Sb_2O_3 (25-100%) nanocomposites and pure Sb_2O_3 nPs were shown in Fig.8. Fig. 7 (a) shows the DSC of pure PPy have broad endothermic peak appeared at around 370.3 °C, this peak reveals the removel of water molecules from the pure PPy molecules. DSC spectrum of pure PPy have sharp exothermic peaks appeared, exothermic peak was shown at about 95.4 °C, which was the complex peak, area of this peak is 756.5 J/g; the onset and endset temperature of the complex peak is 65.2 °C, 110.3 °C respectively, this is presumably due to the polymer decomposition [15].

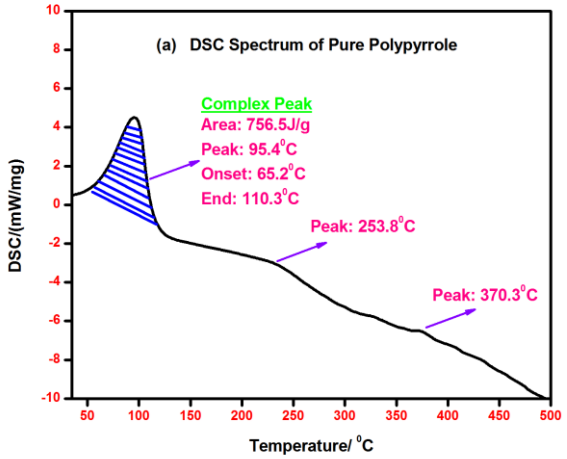

Fig.7a

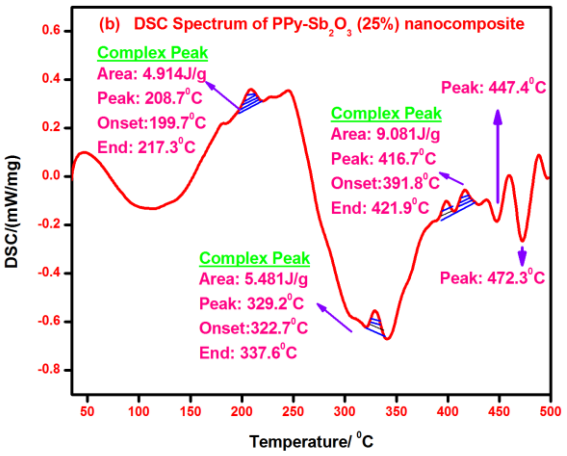

Fig.7b

International Journal of Engineering Research & Technology (IJERT)
ISSN: 2278-0181
Vol. 8 Issue 12, December-2019

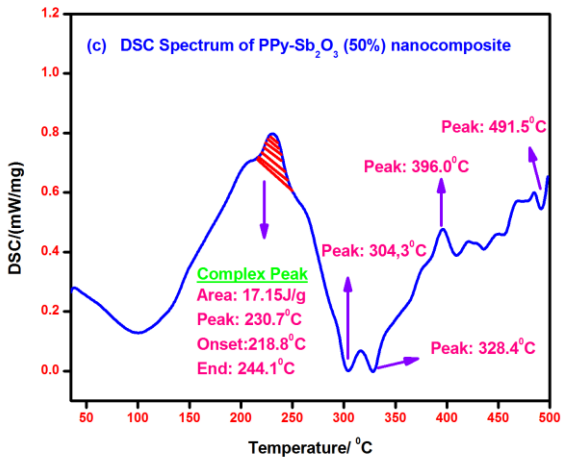

Fig.7c

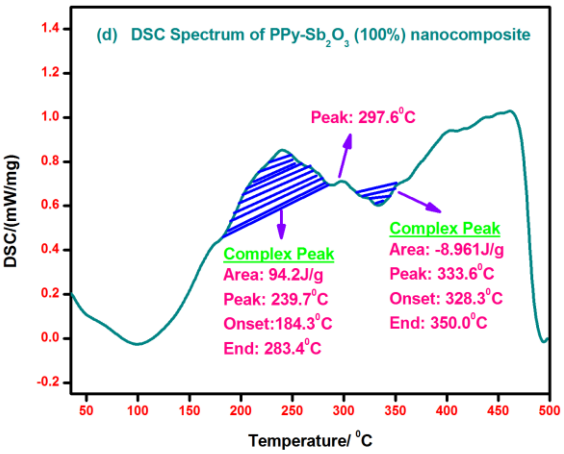

Fig.7d

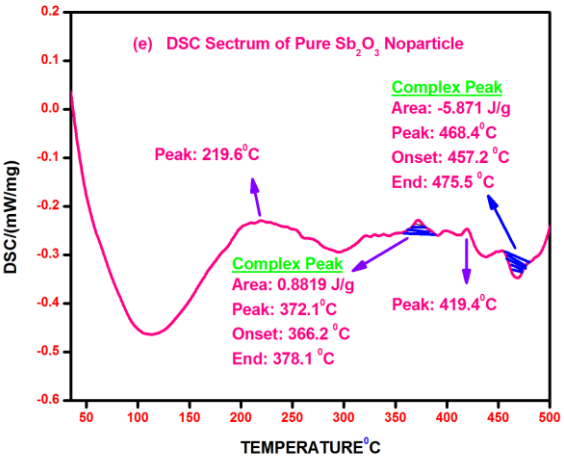

Fig.7e

Fig.7a-7e DSC spectra of pure PPy, PPy-Sb_2O_3 nanocomposites and pure Sb_2O_3 nPs

The DSC spectrum of PPy-Sb_2O_3 (25-100%) nanocomposites is shown in Fig.7 (b-d). The exothermic peaks appeared in the PPy-Sb_2O_3 spectrum which named the complex peaks. From PPy-Sb_2O_3 (25-100%) nanocomposites spectrum which have complex peaks and the area of this complex peaks are 5.481 J/g, 17.150 J/g, and 94.200 J/g. To compare these nanocomposites, the area of the complex peaks is increased with increasing the Sb_2O_3 concentration. The peaks indicating that, the polymer decomposition was found to be present in all ratios (25-100%) of nanocomposites. The peaks indicating that the polymer decomposition was found to be present in PPy-Sb_2O_3 (25-100%), but that was clearly absent in pure Sb_2O_3 nPs samples. Despite the degradation of PPy-Sb_2O_3 (25-100%) nanocomposites samples indicating the gradual enhancement of thermal stability of the polymer chain with increasing the amount of Sb_2O_3. The exothermic peak disappeared for pure Sb_2O_3 sample, indicating strong interaction of the oxide with the polymer chain [16].

4.6. Scanning electron microscopic studies

Scanning electron microscopy (SEM) images of the pure PPy, PPy-Sb_2O_3 (25-100%) nanocomposites and pure Sb_2O_3 nPs are shown in Fig. 8(a-e). The micrographs of pure PPy powder (Fig.8a) show big globular clusters of polymers. The surface morphology of pure PPy changed completely, when it was converted to the nanocomposites with Sb_2O_3 (Fig.8b-d), which established the interaction of Sb_2O_3 surface with the polymer chain. The white colour is Sb_2O_3 nPs and light coloured shell is PPy in the nanocomposites. The prepared nanocomposite exists as relatively loose aggregates of PPy-Sb_2O_3 with crystallize size of 100–250 nm which is observed from SEM study. The amorphous polypyrrole matrix can restrict the further growth of Sb_2O_3 nanocrystals and avoid their further aggregation in the chemical reaction process. According to above results, it can be summarized that, the parameter modulation of PPy in presence of Sb_2O_3 nPs affects not only the final morphology but also the structure of Sb_2O_3 nPs within the PPy-Sb_2O_3 nanocomposites.

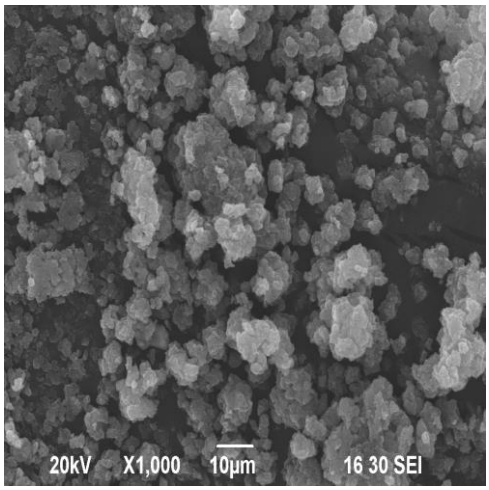

Fig.8a

International Journal of Engineering Research & Technology (IJERT)
ISSN: 2278-0181
Vol. 8 Issue 12, December-2019

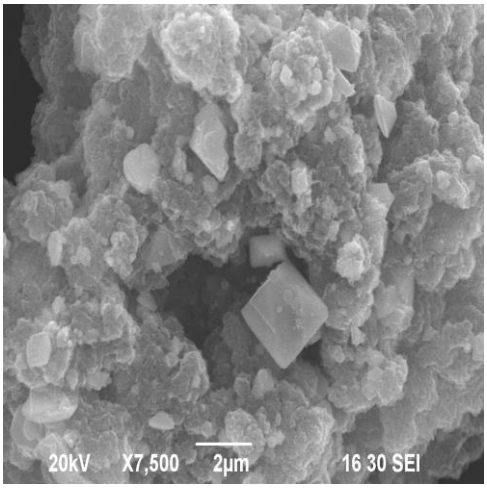

Fig.8b

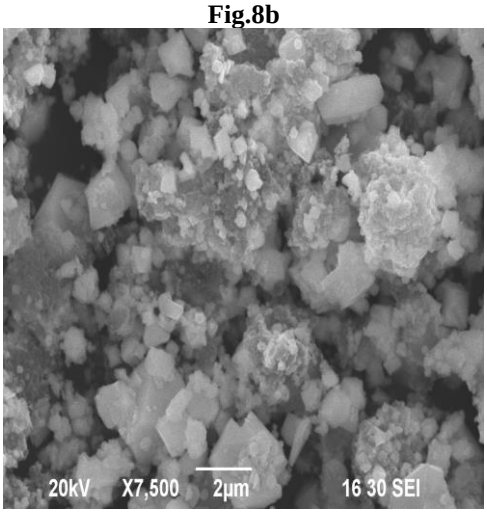

Fig.8c

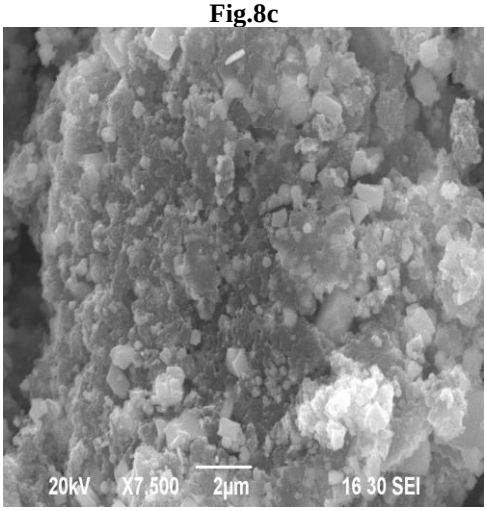

Fig.8d

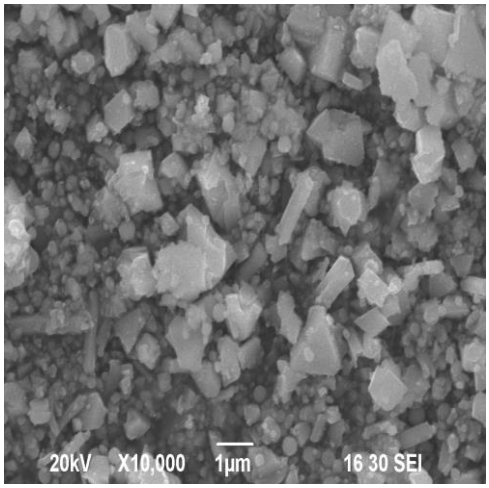

Fig.8e

Fig.8a-8e SEM images of pure PPy (a), PPy-Sb_2O_3 nanocomposites (b,c,d), pure Sb_2O_3 nPs (e)

Succeeded in controlling PPy-Sb_2O_3 morphology, the investigation was turned to explore, the formation mechanism of the PPy-Sb_2O_3 morphology through characterizing the intermediates obtained in different reaction stages. The change in the surface morphology has been observed with increasing composition of Sb_2O_3 (25-100 wt %) in PPy-Sb_2O_3 nanocomposites. The complex, stringy, interconnected network is a general feature of the morphology of PPy-Sb_2O_3 nanocomposites. At higher (100 wt%) of nanocomposites, the connected path way become more and more dense morphology are observed due to excess doping as the PPy-Sb_2O_3 is approached. At this higher percentage of PPy-Sb_2O_3 nanocomposites; the morphology appears almost foam like with PPy-Sb_2O_3 network surrounded by Sb_2O_3. Thus Sb_2O_3 provides large conduction island thereby, reducing the conduction path through the nanocomposites [17].

4.7. Energy dispersive X-ray analysis

Fig. 9(a-e) shows the EDAX spectrum of the pure PPy, PPy-Sb_2O_3 (25-100%) nanocomposites and pure Sb_2O_3 nPs. The corresponding chemical composition is listed in Table.5. Fig.9a illustrates the element weight (%) of C, O, and S of pure PPy sample was 69.32%, 24.24% and 6.44% respectively. It is seen that C, O, S and Sb elements are detected in the PPy-Sb_2O_3 (25-100%) nanocomposites, which indicates that O and Sb-ions have been doped into the PPy matrix successfully. The spectrum of pure PPy, PPy-Sb_2O_3 (25-100%) nanocomposites and pure Sb_2O_3 nPs shows of the carbon molecules weight % are 69.32%, 40.66%, 30.02%, 17.87% and 14.80% which is element composition in which decreasing trend is appeared for the same element composition changes were obtained for oxygen and sulfur molecules weights, and the weight % of antimony ion are 35.72 %, 49.98 %, 62.05 % and 85.20 %, for this chemical composition increasing trend was appeared. As shown in Fig.9b an element like carbon, sulfur, oxygen and antimony of PPy-Sb_2O_3 nanocomposite samples which compare due to pure PPy, the element contents of carbon, oxygen and sulfur was decreased,

International Journal of Engineering Research & Technology (IJERT)
ISSN: 2278-0181
Vol. 8 Issue 12, December-2019

Antimony alone increased with increasing the concentration of Sb_2O_3 nanoparticles [18].

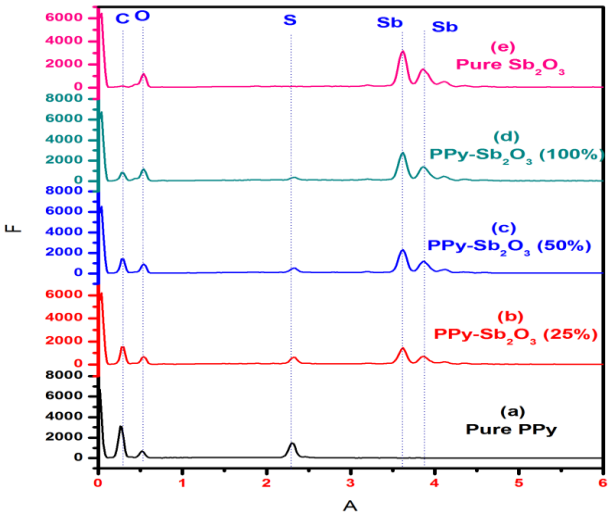

Fig.9 EDAX spectra of pure PPy (a), PPy-Sb_2O_3 nanocomposites (b,c,d) and pure Sb_2O_3 nPs (e)

Sample Name	Weight (%)				
	Carbon	Oxygen	Sulfur	Antimony	Total
Pure PPy	69.32	24.24	6.44	-	100
PPy-Sb_2O_3 (25%)	40.66	19.60	4.02	35.72	100
PPy-Sb_2O_3 (50%)	30.02	17.35	2.65	49.98	100
PPy-Sb_2O_3 (100%)	17.86	18.24	1.85	62.05	100
Pure Sb_2O_3	14.80	-	-	85.20	100

Table.5 Element analysis data of pure PPy, PPy-Sb_2O_3 nanocomposites and pure Sb_2O_3 nPs

The element contents of PPy-Sb_2O_3 (25-100%) nanocomposites show a higher Sb contents due to the formation of a large amount of Sb_2O_3.

5. Conclusion

The FTIR analysis is carriedout for pure PPy, Sb_2O_3 nPs and PPy-Sb_2O_3 (25-100%) nanocomposites systematically. The characteristics bands were observed for the corresponding materials. From the results, one can conclude that, the wavenumber region is shifted to higher values after Sb ion absorption. The results indicate that the co-ordination bond formed between the long pair of electrons of the atom in the PPy chain with the orbit of Sb atom of Sb_2O_3, indicating the strength of PPy-Sb_2O_3 nanocomposites have been synthesized successfully and the observed shift which indicates the interaction between PPy and Sb_2O_3 nPs. UV-visible spectra results indicates that the absorption bands which are correspond to the transition of π-π*. From the tauc plot, one can conclude that the band gap energy is calculated for each case of materials. Among the materials, the band gap energy (3.46 eV) is obtained for pure PPy. The band gap is decreased with increasing Sb_2O_3 concentration and this indicates the PPy-Sb_2O_3 interactions are significantly increased by increasing the Sb_2O_3 concentration loading to reduce the energy level intervals. X-Ray diffraction studies suggest the crystallographic nature of the materialsand from the report, we analyze the XRD patterns of pure PPy, Sb_2O_3 nPs and PPy-Sb_2O_3 nanocomposites is in a systematic manner. The amorphous peak of pure PPy was appeared in addition to sharp peak, but the other patterns indicates the crystalinity was greatly improved the with addition of Sb_2O_3 form the nanocomposites. From the crystallite size calculations, the average crystallite size of PPy-Sb_2O_3 (25 wt%), PPy-Sb_2O_3 (50 wt%) and PPy-Sb_2O_3 (100 wt%) are 97 nm, 170 nm and 176 nm respectively. From this, one can inferred that the lowest average crystallite size is observed for PPy-Sb_2O_3 (25%). The strain and dislocation density calculation and the data suggest the crystallographic nature and defects of the materials. Thermogravimetric results of the pure PPy, Sb_2O_3 nPs and PPy-Sb_2O_3 (25-100%) nanocomposites suggest that thermal behavior and stability of the materials and the number of stages of decomposition may vary depending upon the materials. In this report, the lowest number of stages (2) is observed for pure PPy. The residual mass of PPy-Sb_2O_3 (25-100 wt%) is increased, when the composition increase from PPy-Sb_2O_3 (25 wt%) to PPy-Sb_2O_3 (100 wt%). This is because, the increase of loading amount of Sb_2O_3 in the matrix of PPy, but the residual temperature is almost constant for all the cases. From the differential scanning calorimetric analysis, one can reveal the stages in which the molecules of various categories eliminating from the surface. The exothermic and endothermic peaks suggests that the polymer decomposition is found in the case of PPy-Sb_2O_3 nanocomposites. These kinds of analysis help us to estimate the thermal stability of pure PPy, Sb_2O_3 nPs and PPy-Sb_2O_3 (25-100%) nanocomposites. In this report, the surface morphological analyses of pure PPy, Sb_2O_3 nPs and PPy-Sb_2O_3 (25-100%) nanocomposites are carriedout successfully. Actually, the particles are not in spherical in size for the all the cases. Instead, the particles are agglomerated initially and the some square shaped particles are also found and also there are some surface modifications, due to the agglomeration of the particles, so that the core shell like structure is formed on the surface of PPy matrix and this can be seen clearly from the morphological data. From the EDAX analysis, the elemental composition of pure PPy, Sb_2O_3 nPs and PPy-Sb_2O_3(25-100 wt%) is estimated clearly. From the increasing trend of antimony, one can inferred the loading amount of Sb_2O_3 in the matrix of PPy. This kind of analysis helps us to gain more information about the structure and behavior of the materials.

International Journal of Engineering Research & Technology (IJERT)
ISSN: 2278-0181
Vol. 8 Issue 12, December-2019

REFERENCES

[1] Li Cui, Juan Li, Xiao-gang Zhang. Materials Letters 63 (2009) 683-686.
[2] Pi-Guey Su, Lin-Nan Huang. Sensors and Actuators B 123 (2007) 501-507.
[3] Yu Xiea, Xiaowei Hong, Yunhua Gao, Mingjun Li, Jinmei Liu, Juan Wang, Jing Lu. Synthetic Metals 162 (2012) 677-681.
[4] Komilla Suri, S. Annapoorni, R.P. Tandon, N.C. Mehra. Synthetic Metals 126 (2002) 137-142.
[5] Komilla Sari, S.Annapoorni, A.K.Sarkar, R.P.Tandon. Sensors and Actuators B 81 (2002) 277-282.
[6] Ze Hua Dong, Yan Li Wei, Wei Shi, Guo An Zhang. Materials Chemistry and Physics 131 (2011) 529-534.
[7] Madhumita Bhaumik, Arjun Maity, V.V. Srinivasu, Maurice S. Onyango. Journal of Hazardous Materials 190 (2011) 381-390.
[8] Sukanta De, Ashis Dey, S.K. De. Solid State Communications 137 (2006) 662-667.
[9] Kousik Dutta, S.K. De. Solid State Communications". 140 (2006) 167–171.
[10] Debabrata Nandi, Arup Kumar Ghosh, Kaushik Gupta, Amitabha De, Pintu Sen, Ankan Duttachowdhury, Uday Chand Ghosh. Materials Research Bulletin 47 (2012) 2095–2103.
[11] Wenqin Wang, Wenli Li, Ruifeng Zhang, Jianjun Wang. Synthetic Metals 160 (2010) 2255-2259.
[12] Haldorai Yuvaraj, Eun Ju Park, Yeong-Soon Gal, Kwon Taek Lim. Colloids and Surfaces A: Physicochem. Eng. Aspects 313-314 (2008) 300-303.
[13] Manawwer Alam, Anees A. Ansari, Mohammed Rafi Shaik, Naser M. Alandis. Arabian Journal of Chemistry (2012).
[14] Emine Temizel, Esra Ayan, Mehmet S¸ enel, Hamit Erdemi, Mustafa S. Yavuz, Huseyin Kavas, Abdulhadi Baykal, Ramazan Ozturk. Materials Chemistry and Physics 131 (2011) 284-291.
[15] Hamid Heydarzadeh Darzi, Saeedeh Gilani Larimi, Ghasem Najafpour Darzi. Synthetic Metals (2011).
[16] S.Y. Chew, Z.P. Guo, J.Z. Wang, J. Chen, P. Munroe, S.H. Ng, L. Zhao, H.K. Liu. Electrochemistry Communications 9 (2007) 941–946.
[17] C. Lai, G.R. Li, Y.Y. Dou, X.P. Gao. Electrochimica Acta 55 (2010) 4567-4572.
[18] Madhumita Bhaumika, Taile Yvonne Leswifia, Arjun Maity, V.V. Srinivasu, Maurice S. Onyango. Journal of Hazardous Materials 186 (2011) 150–159.